Nat. Hazards Earth Syst. Sci. Discuss., 1, 1823–1855, 2013
www.nat-hazards-earth-syst-sci-discuss.net/1/1823/2013/
doi:10.5194/nhessd-1-1823-2013

Natural Hazards and Earth System Sciences
Open Access
Discussions

Tsunami hazard in La Réunion island from numerical modeling of historical events

E. Quentel[1], **A. Loevenbruck**[1], **H. Hébert**[1], **and S. Allgeyer**[1,*]

[1]CEA, DAM, DIF, 91297 Arpajon, France
[*]now at: The Australian National University, Research School of Earth Sciences, Canberra 0200, Australia

Received: 15 March 2013 – Accepted: 3 April 2013 – Published: 8 May 2013

Correspondence to: E. Quentel (elisequentel@gmail.com)

Published by Copernicus Publications on behalf of the European Geosciences Union.

Abstract

Whereas major tsunamis have recently affected the southwest Indian Ocean, tsunami hazard in this basin has never been thoroughly examined. Our study contributes to fill in this lack and focuses on La Réunion island for which tsunami hazard related to great earthquakes is evaluated by modeling the scenarios of major historical events. Then, our numerical modeling allow us to compare the tsunami impact at regional scale according to the seismic sources; we thus identify earthquakes locations which most affect the island and describe the impact distribution along its coastline. Thirdly, detailed models are performed for selected sites based on high resolution bathymetric and topographic data; they provide estimations of the water currents, wave heights and potential inundations. When available, field measurements and tide records allow testing our models. Arrival time, amplitude of the first wave and impact on the tide gauge time series are well reproduced. Models are consistent with the observations. The west coast of La Réunion is the most affected (to 2.7 m in the harbour of Le Port Est for 2004 event) by transoceanic tsunamis. Numerical modeling has been performed at Saint-Paul for the 2004 Sumatra-Andaman event and 1833 Sumatra event; the low topography of this town could make it vulnerable to tsunami waves. Harbours, particularly prone to undergo significant damages, are also examined. Outside the harbours as well as at Saint-Paul, inundations are predicted along the coastline due to important local wave heights (> 2.5 m).

1 Introduction

Recent tsunamigenic earthquakes in the Indian Ocean (Sumatra, 26 December 2004 and Java, 17 July 2006) (Okal et al., 2006) highlighted the tsunami hazard on the Mascarene archipelago to which the French island of La Réunion belongs (Fig. 1). Okal and Synolakis (2008) have shown that waves with amplitudes higher than those due to the great 2004 event may be generated by subduction mega-earthquakes, especially

NHESSD
1, 1823–1855, 2013

in case of scenarios similar to the 1833 Sumatra tsunami. Far-field tsunami hazard assessment is thus crucial for these islands of the Indian Ocean. Seven events have been recognized to have impacted La Réunion in the past: Krakatau 1883, Sumatra 1907, Sumatra 2004, Sumatra 2005, Java 2006, Mentawai 2007, and Mentawai 2010. The effects of these teletsunamis were mostly concentrated on the western shore of the island (Sahal et al., 2011). The most impacting identified event was due to the 1883 Krakatau's second blast, collapse of the Danan peak and formation of its caldera (Choi et al., 2003), with run-up values reaching 7 m in Saint-Paul. This flooding was probably due to an atmospheric coupling infered to the blast and not due to the tsunami. A height of 1.72 m related to the most recent tsunami, after the 25 October 2010 earthquake ($M_w = 7.7$), was reported in Sainte-Marie (Sahal and Morin, 2012). The 2004 event was well recorded on a wide variety of instruments and sensors, including conventional coastal tide gauges (Merrifield et al., 2005; Rabinovich et al., 2007) and outstanding observations (Okal et al., 2006; Sahal et al., 2011). Mapping of the flooded areas documented by run-up measurements (Okal et al., 2006) allows defining the 2004 tsunami impact on the Mascarene islands. Thanks to the survey of Okal et al. (2006) in La Réunion after the 2004 event, run-ups have been measured in different harbours: 2.4 m for Saint-Gilles (west coast of the island), 2.7 m for Le Port (harbour of Le Port Est) (west coast), 2.0 m for Sainte-Marie (north coast), 1.4 m for Saint-Pierre (south coast) and 2.0 m for Sainte-Rose (east coast). In this study, numerical modeling of past earthquakes triggered events contributes to quantify the potential impact of tsunamis on La Réunion. We chose tsunamigenic earthquakes located along all subduction zones in the Indian Ocean to determine which zones potentially generate great far-field tsunamis for La Réunion. We keep four earthquakes (1833, 1945, 2004 and 2006) with magnitude greater than $M_w = 7.7$. As a first step, we conduct a rapid historical analysis with numerical modeling to determine the regional impact and the great tsunami. The available data provides essential insights into the historical catalogue of recorded run-ups (Sahal et al., 2011). Then, we select the two great earthquakes of 1833 and 2004 to model the major tsunami impact on specific areas. Le Port and

NHESSD
1, 1823–1855, 2013

Saint-Paul are located in the western part of La Réunion where tsunamis are the most powerful and where most of damage have been observed. These towns have been selected for their inherent environmental and human potential issues. About hundred thousand people live in Saint-Paul and about forty thousand in Le Port. These towns have coastal typology characterized by beaches, coastal housings and two basins for Le Port. Finally, we map the flooded and protected areas in those two towns.

2 Tsunami modeling approach

Tsunamis are long waves propagating across the ocean triggered by earthquakes or landslides. Due to their long wavelength they can be described following the classical, non-linear shallow-water theory (Heinrich et al., 1998; Hébert et al., 2007). The source is treated as an instantaneous perturbation of the seabottom in response to a static displacement due to an earthquake. The initial deformation is modeled by a dislocation embedded in elastic space (Okada, 1985). This model is constrained to satisfy the seismic moment M_0:

$$M_0 = \mu \cdot U \cdot L \cdot W \tag{1}$$

where μ is the rigidity, U the slip amount, L and W the length and the width of the fault.

The total initial displacement provides the initial condition to solve the hydrodynamic equations. These equations describe the mass (Eq. 1) and momentum (Eq. 2) conservation.

$$\frac{\partial(\eta + h)}{\partial t} + \nabla \cdot (\boldsymbol{u}(\eta + h)) = 0. \tag{2}$$

$$\frac{\partial \boldsymbol{u}}{\partial t} + (\boldsymbol{u} \cdot \nabla)\boldsymbol{u} + f\boldsymbol{u} = -g\nabla\eta \tag{3}$$

where h is the sea depth, η is the water elevation above mean sea level, $\boldsymbol{u}$ is the depth-averaged horizontal velocity vector, g is the gravitational acceleration, and f are the external forces.

NHESSD
1, 1823–1855, 2013

Equations of mass and momentum conservation are solved in spherical coordinates by means of a finite-difference scheme of Crank and Nicolson (1947), centered in time, and with use of an upwind scheme in space. Under the shallow-water theory, dispersive effects are neglected. The velocity $c = \sqrt{g \cdot h}$ drastically decreases close to the coast where the shoaling effect leads to wave amplification. The decreasing tsunami wavelength near the shoreline requires finer bathymetric grids. Open free-boundary conditions are applied to the boundaries of the largest and coarsest grid, whereas wave heights and velocities along the boundaries of each fine grid are spatially interpolated at each timestep from the values computed in the coarser grid that contains it. This model has been tested and validated in numerous cases (e.g. Hébert et al., 2001; Sahal et al., 2009).

3 Scenarios of tsunamis from historical earthquakes triggered events

In the Indian Ocean, as illustrated by the great M_w = 9.2 2004 Sumatra-Andaman event (Lay et al., 2005; Hébert et al., 2007; Sladen and Hébert, 2008), earthquakes along the subduction zones (Fig. 1) are the main sources of tsunamis that are prone to propagate across the Indian Ocean and reach, 5000 km further away, La Réunion.

Based on their review of on-line and previously published regional databases (Dunbar, 2010; Rastogi and Jaiswal, 2006) and on their field investigations, Sahal et al. (2010) compiled a catalog of tsunamis for the Indian Ocean; potentially tsunamigenic earthquakes are described as well as the past events and the territories, such as La Réunion island, that they have struck. The Indian Ocean undergone tsunamis triggered by Sumatra, Java and Makran subduction earthquakes. Whereas observations show that events generated along the Sumatra and Java islands reached La Réunion over the past, there is no evidence of impact related to sources from the Makran, such as the 1945 earthquake (M_w = 8.1). We however examine the tsunamigenic potential of all subduction zones in order to define which are prone to generate the most destructive waves for La Réunion. We hence focus on two earthquakes that occurred in Sumatra

NHESSD
1, 1823–1855, 2013

(24 November 1833 and 26 December 2004), one in Java (17 July 2006), but also simulate the 27 November 1945 Makran event.

3.1 The earthquake of 24 November 1833

The great 24 November 1833 earthquake occurred along the Sumatra subduction zone near the Pagai islands (Zachariasen et al., 1999; Jaiswal et al., 2008; Natawidjaja et al., 2006) with an estimated magnitude of $M_w = 9.2$ ($M_0 = 7.15 \times 10^{22}$ Nm). Its estimated position is: 3° S, 99.5° E with a depth of 10 km. The seismic source determined by Zachariasen et al. (1999) provides the largest seismic moment suggested by studies Natawidjaja et al. (2006), with a rupture length of 550 km and a width of 250 km. The source parameters used for the model are shown in Table 1. However nothing similar to any tsunami has been recorded in La Réunion. The lack of archive for this period could explain why, but also no corresponding tsunami deposits have been identified. Damage related to this transoceanic tsunami is mentioned in only one report which includes a single observation in the Seychelles (Okal and Synolakis, 2008).

The focal mechanism is based on studies of sediments and corals along the Pagai islands (Zachariasen et al., 1999; Natawidjaja et al., 2006). This great earthquake has created a strong surrection of the Pagai islands, which illustrates the proximity of islands from the oceanic trench. The tsunami generated by this earthquake constitutes a worst-case event in the Indian Ocean that we use to know the maximum impact on the island of La Réunion.

3.2 The earthquake of 26 December 2004

Widely studied, the 26 December 2004 Sumatra-Andaman earthquake generated a catastrophic tsunami causing more than 200 000 casualties, not only in northern Sumatra, but also in remote places, from Thailand, Sri Lanka, to east Africa (namely Somalia). The faulting spread over more than one thousand of kilometers along the Sumatra subduction zone with a magnitude $M_w = 9.2$. We used two different source

NHESSD
1, 1823–1855, 2013

models. The first model corresponds to the Model A of Hébert et al. (2007). This model is subdivided in six elementary fault planes with a common central depth of 20 km and an heterogeneous displacement between 3 and 12 m providing a seismic moment of $M_0 = 6.76 \times 10^{22}$ Nm. The second model is taken from Sladen and Hébert (2008) with a seismic moment of $M_0 = 2.54 \times 10^{22}$ Nm. The earthquake occurred at 00:58 UTC (local time being UTC + 4 h). The tide gauge data from La Pointe des Galets harbour gives us some clues to validate our model for 2004 event, as well as historical earthquakes. Thanks to the survey of Okal et al. (2006) in La Réunion after the 2004 event, some eyewitnesses note that the successive waves reached the coast, starting early afternoon til evening, with a waves frequency's around 20 min. The most spectacular effect of the tsunami was the double breaking of the moorings tying up a container carrier in Le Port Est four hours after the first arrival. The recent 2010 Mentawai event which occurred during the night also produced many damages: boats sunk on harbours of Sainte-Marie and Saint-Gilles. Two meters of maximum sea level have been observed by witnesses in Sainte-Marie. The effects of the tsunamis of 2004 and 2010 ($M_0 = 4.16 \times 10^{20}$ N.m defined by USGS) are mainly concentrated in harbours where they damaged many boats.

3.3 The earthquake of 27 November 1945

The Makran subduction zone (MSZ) is an active seismic area (Byrne et al., 1992; Pararas-Carayannis, 2006). This subduction zone is known for its major transpressional strike-slip with a slow moving subduction zone (40 mm an^{-1}) and a dip angle between 2° and 8° (Kopp et al., 2000; Schläter et al., 2002). The study of Jackson and McKenzie (1984) shows that the earthquakes located under 20 km deep are likely to generate tsunamis. Few authors have studied the earthquake of 27 November 1945 with a magnitude estimated to $M_w = 8.1$ (Rajendran et al., 2008; Heidarzadeh et al., 2007). This is a pretty large earthquake and it caused an important tsunami on the coastlines of India and Pakistan. However, no tsunamis records have been observed in

NHESSD
1, 1823–1855, 2013

La Réunion. To determine the tsunami impact on La Réunion, we have used the source parameters of Rajendran et al. (2008) with a seismic moment of $M_0 = 1.54 \times 10^{21}$ Nm.

3.4 The earthquake of 17 July 2006

The 17 July 2006 earthquake which occurred on the Java subduction zone triggered a tsunami that propagated at least as far away as La Réunion. The hypocenter has been localized at 10.28° S, 107.78° E and 34 km depth. Being given the large tsunami with respect to the magnitude, this event was defined as a tsunami earthquake, as confirmed later by seismological studies (Ammon et al., 2006). We use the USGS source model which consists of 179 subfaults and describes a complexe heterogeneous slip distribution. The magnitude of this earthquake is estimated to $M_w = 7.7$, the seismic moment is $M_0 = 3.98 \times 10^{20}$ Nm.

4 Global impact analysis

As a first step, we examine the impact of each event at the basin scale (Fig. 2); the radiation pattern gives an overview of the relative tsunami energy for each scenario. The 1833 model predicts the largest impact offshore. Tsunamis generated along the Sumatra subduction zone (1833 and 2004 events) reach La Réunion in 7 h. The 1833 tsunami travels through the Indian Ocean and reached Burma, Sri lanka, India and Bangladesh in 3 h, then Australia in 5 h and Oman, Yemen, Somalia and finally Pakistan in 6–7 h. The reliefs of the Chagos-Laccadives ridge influence the propagation of tsunami and create diffractions (Fig. 2). For the 2004 event, this ridge diffracts the waves and changes their direction towards the west. Mascarene Plateau is most protected due to this diffraction, but maximum amplitude is around 1 m along the plateau as La Réunion island. We observe the same results for the two models (Hébert et al., 2007; Sladen and Hébert, 2008). Based on the source parameters, the 1833 event (Zachariasen et al., 1999) model is considered as showing the maximum tsunami

NHESSD
1, 1823–1855, 2013

impact coming from Sumatra subduction zone La Réunion could undergo (Fig. 2). Since the earthquake is located further south than the 2004 event, the tsunami spreads more to the south–west. The wave arrival is more directly oriented towards the island. Tsunami is not diffracted by sea bottom reliefs. Maximum amplitude in the Mascarene Plateau is around 2 m. South Madagascar is also very affected by the tsunami with the same maximum amplitude.

Modeled tsunamigenic earthquakes along the Java and Makran subduction globally lead to a smaller impact, but they still could produce locally 1 m high waves along the first 500 km of propagation. The simulation of the 1945 tsunami does not predict any significant amplitude. For the 2006 event, a weak tsunami reaches the island with 20 cm waves after 7.5 h of propagation.

We focus on both earthquakes along the Sumatra subduction zone that induced the strongest tsunamis, i.e. the 2004 ($M_w = 9.2$) and 1833 ($M_w = 9.2$, assumed) events. Because of the source location, they both strongly struk the island; the 1833 scenario leads to the maximum tsunami impact.

For these two events, the tsunamis come from the north–east and are trapped around La Réunion, producing two fronts of edge waves that join on the leeward side of the island, more precisely at La Pointe de Saint-Gilles promontory. This could explain the large water heights that have been observed there, 5 m in 1833 and 1.5 m in 2004 (Okal et al., 2006) (Fig. 3).

5 Detailed study sites

To properly model the tsunami waves at small scale we used eight nested bathymetric grids with increasing resolution, from 3 arc minutes in the deep ocean to 4 or 3 m locally (Fig. 4). GEBCO (General Bathymetric Chart of the Oceans) provides the global bathymetry; the high resolution data were extracted from the SHOM (Service Hydrographique et Océanographique de la Marine) DDE (Direction Départementale de l'Equipement) database. The SHOM data cover the surrounding area of the island

NHESSD
1, 1823–1855, 2013

within 30 km from the coastline. The spatial step lies between 100 m and 500 m. The DDE data, with the best resolution (8–25 m), document the harbours. The finest grids where flooding is computed include high resolution topographic data (better than 5 m) from the Litto3D project. Our grids set is built for the detailed study of three sites: the town of Saint-Paul and the two harbours of Le Port, which are separated by the promontory of La Pointe des Galets. These places have been chosen for their location (on the western coast along which a larger tsunami impact is expected) and for their human vulnerability. The town of Saint-Paul is located on the west coast of the island, north of Saint-Gilles. It extends from the beach to the main road, 650 m further to the East. To the north, a swamp area, called L'Etang, passes through the town (Fig. 4). The nearshore bathymetry gradually decreases before giving way to the continental slope. The location, the important coastal people density (100 000 inhabitants) and the low elevation of many areas (< 5 m) of Saint-Paul point out a high vulnerability that may lead to a high tsunami risk. The resolution of the final Saint-Paul grid is 4.63 m. The harbours of Le Port are described by two distinct 3 m resolution grids (Fig. 4), which take into account the recent modifications following work undertaken in early 2010. The harbour of La Pointe des Galets, west-facing, is composed of a main basin and two secondary, one to the South housing the marina, and one to the North where the tide gauge is located (lat: −20.935, long: 55.28). The neashore slope is relatively irregular, cut by small submarine canyons, one extending into the acces channel of the harbour. The 10 m deep bottom of the basins are almost flat. The north-facing harbour, Le Port Est, is fringed by a gentle nearshore bathymetric slope. It is composed of a main basin with an extension to the west. The entrance is bordered by two seawalls. For both harbours, buildings are about 2 m a.s.l.

NHESSD
1, 1823–1855, 2013

6 Results: impact on La Réunion

6.1 La Pointe des Galets tide gauge record

The harbour of La Pointe des Galets is equipped with a tide-gauge since 1974; following the great 2004 Sumatra event, a new instrument has been installed in mid-2007. After filtering the tide, whose frequency is estimated to 4×10^{-5} Hz, the tsunami signal recorded in 2004 (Fig. 5) allows us to determine the arrival time, the amplitude and the periodicity of the waves. The first arrival was registered at 12:00 LT. With a maximum of 20 cm, it was not the strongest wave; amplitudes up to 30 cm have been recorded during the first two hours and waves, whose periodicity is estimated to 15 min, remained significant during at least 8 h.

In order to compare our models to this record, the synthetic signal is extracted from our simulations with the sample rate of the 2004 tide-gauge (i.e. 2 min).

The first synthetic tidal modeling for the model of Sladen and Hébert (2008) shows a correlation in time and amplitude (Fig. 5) with the real signal. The first wave is well modeled. The model shows an arrival of the following wave 5 min in advance. The modeled amplitude is 10 cm stronger for the fourth and fifth waves.

The second model based on Hébert et al. (2007) shows a better correlation in time (Fig. 5), but the first wave arrives 5 min too late. Apart from the first wave whose amplitude is properly reproduced, maximum wave heights are largely overestimated.

The significant differences between the two synthetic signals highlight the high sensitivity of tsunami impact to the source model, even in the far-field. This suggests that the limited fit to the observed tidal record might be related to source model imprecision. We note that the complex source with multiple subfaults from Sladen and Hébert (2008) more properly reproduces the real signal than the six subfaults seismic source from (Hébert et al., 2007). For both models, after two hours of propagation, synthetic signals differ too much from the measurement and cannot be compared.

NHESSD
1, 1823–1855, 2013

No observations were available for the 1833 event. Through numerical modeling, the tsunami signal can be predicted at the tide gauge of La Pointe des Galets (Fig. 5). Using a simple seismic source (Zachariasen et al., 1999), the modeled waves are higher than during the 2004 event, with a first maximum of about 100 cm. The amplitude crest to trough is twice as large in the case of the 1833 simulation (−150 cm–100 cm) as for the 2004 one (about −50 cm–50 cm). This 1833 scenario is based on the hypothesis of a strong tsunamigenic earthquake described by a simple source model; hence it provides a worst-case scenario.

Numerical results are interpreted with the model of Sladen and Hébert (2008) for the 2004 event and with the model of Zachariasen et al. (1999) for the 1833 event. This interpretation is limited to 2 h after the first arrival. We use the information of maximum wave height, maximum velocity, the velocity field and the run-up that we could determine. We only show the maximum wave heights for the 2004 event (Fig. 6) for comparison with the 1833 event (Fig. 7). As 1833 event is a worst-case event, we concentrate our study on the results of this event.

6.2 Amplification areas

Around the island, the bathymetric plateau amplifies the waves and generates maximum wave heights where flooding could be observed, as illustrated on Fig. 3 for the 2004 scenario. More locally, the 2004 and 1833 scenarios predict amplification areas in the vicinity of La Pointe des Galets; the largest waves (3.5 m for 2004 and 10 m for 1833) are modeled East of Le Port and at the promontory of La Pointe des Galets (1 m for 2004 and 6 m for 1833) (Figs. 6-right and 7). In Saint-Paul bay, some amplification to the South may be attributed to the wave trapping that lead two wave fronts to join on this western area of the island.

NHESSD
1, 1823–1855, 2013

6.3 Tsunami impact on the harbours

6.3.1 harbour of La Pointe des Galets

On both sides of the harbour entrance, the coastline is struck by large waves up to about 1.5 m high for 2004 (Fig. 6) and 4 m high for 1833 (Fig. 8). Larger water heights are expected to the north, this amplification may be related to the shallow bathymetric area off the coast (Fig. 4).

The harbour is well protected with a height of less than 50 cm in 2004 but is less protected for the 1833 scenario with a height of 3 m (Fig. 8). The maximum velocities are consistent in the amplification zone but not in the basins. On the coastline, velocities lay between 5 $m s^{-1}$ and 10 $m s^{-1}$ but in the basin velocities reach around 2 $m s^{-1}$ with strongest velocities at the entrance of basins (around 5 $m s^{-1}$). Off this harbour, the northern coast exhibits maximum wave heights associated with high velocities; therefore, we consider that this coast could be flooded by the waves during a major event similar to the 1833 scenario.

6.3.2 harbour of Le Port Est

For Le Port Est, significant currents are modeled in the entrance channel and along the East coast where largest amplitudes are expected (Fig. 9). Maximum wave height is 6 m outside the harbour. Inside, the waves are globally smaller, but amplitude up to 5 m is modeled south of the main basin.

6.3.3 Flooding

Flooding is limited to the beaches along the coasts of these harbours and to the extremities of the basins for the 1833 scenario. In any case, the flooding is limited to 2 m of run-up. All buidings which are located above 2 m height are not reached by the waves. The maximum run-up modeled to the East coast (outside the harbour) for the 1833 event is 6 m high. The horizontal extent of flooding is about 50 m. For the 2004

NHESSD
1, 1823–1855, 2013

scenario, the flooding along the the East coast is limited, with a run-up of around 2 m, an horizontal flooding extent of 20 m and a mean flow depth of 50 cm.

6.3.4 Currents in harbours

The most important impact observed during the 2004 event was the disturbance created in the harbours by strong velocities. The most spectacular example was the double breaking of the ropes tying up a container carrier, four hours after the first arrival in Le Port Est. In all models, currents are strong in harbours with sometimes the appearance of an eddy. In the northern basin of La Pointe des Galets harbour, we modeled circular maximum velocities for the 1833 event forming an eddy-like feature. These circular velocities are due to local vorticity in this basin.

In 2004, modeled currents in the basin of Le Port Est were around $1\,m\,s^{-1}$. These currents are consistent with the breaking of the moorings. For the 1833 scenario, velocities in the harbour are also of the order of $0.5\,m\,s^{-1}$ but two turbulent eddies with $1\,m\,s^{-1}$ are created in the main basin (Fig. 10). These eddies are consistent with observed eddies formed by tsunamis waves elsewhere in the world like that of the 2011 Tohoku event in the Oarai Port in the Ibaraki province (http://storage.canalblog.com/88/61/169396/63073616.jpg) (Lynett et al., 2012). Understandably, this phenomenon can produce important damages to ships at La Réunion. Currents in the entrance of harbours are also strong: around $3\,m\,s^{-1}$. Though flooding is limited in these harbours, the strong currents are the most important consequence of such tsunamis for La Réunion Island. Strong currents ($1\,m\,s^{-1}$) are found in all of our models (1833, 2004).

6.4 Tsunami impact on Saint-Paul

The coastline of Saint-Paul did not react to the tsunami in the same way as harbours. The southern bay is the most affected due to junction of the two fronts of the tsunami. The wave height is around 3.5 m in 2004 (Fig. 6) and 8 m for the 1833 scenario (Fig. 11). These heights are consistent with a maximum velocity of $15\,m\,s^{-1}$ in the south whereas

NHESSD
1, 1823–1855, 2013

the wave height was 2 m near the Raviva Bernica in 2004 and 4 m for the 1833 scenario. In 2004, flooding was limited to the beaches. The alongshore bar protects the town. For the 1833 model, the waves are too high for this natural barrier. The southern districts of the city are flooded. A wave height profile in the southern coast shows the water going across the 4 m high alongshore bar (Fig. 12). The modeled run-up is 7 m with a flooding distance of 600 m.

7 Discussion: protected and liable to flooding areas

Our models allow us to determine which areas are protected or liable to inundation. The eastern coast of the island is generally protected, opposite of the western coast which is under the influence of the junction of the two fronts of the tsunami. The maximum amplitude observed by Okal et al. (2006) between 0.9 m and 2.30 m west of La Réunion is consistent with our modeled maximum amplitude. A run-up of 2.7 m was observed in 2004 in the harbour of Le Port Est which is close to our value (2 m in Le Port Est). In the 3 studied places (Saint-Paul, Le Port Est and La Pointe des Galets harbours of the city of Le Port), we identified sites vulnerable to tsunamis. Maximum wave height and inundation are determined along the east coast of Le Port Est and north coast of La Pointe des Galets harbour. The tsunami waves are amplified in these places due to a bathymetric plateau which can induce an increase of the waves causing flooding. In the south of Saint-Paul, we also have an amplification phenomenon with maximum wave height (8 m) and flooding (run-up = 7 m) for the 1833 event due to the junction of the two fronts of the tsunami. In all our models, this area exhibits wave heights and flooding when the tsunami is strong and well oriented (propagation to the south–west when the seismic source is located on the Sumatra subduction zone). The flooding is limited to the beaches when the tsunami is smallest or when it is not properly oriented like in 2004 and in 2006 (tsunami propagation to the west). Saint-Paul is protected to tsunamis by an alongshore, 4 m high, bar, but for the worst-case scenario, waves pass across the alongshore bar. The southern districts are flooded. In the harbours basins,

NHESSD
1, 1823–1855, 2013

flooding is limited to 2 m high and does not reach the buildings. The two studied events show strong currents in harbours and flooding on beaches. In the worst case (1833 event), we modeled the appearance of turbulent eddies in the harbour of Le Port Est and the flooding of the southern districts of Saint-Paul.

8 Conclusions

The last tsunamis in the Indian Ocean (2004, 2010) reached La Réunion with damages to ships in the harbours. These tsunamis put in evidence the lack of information on tsunami hazard on this island. With the modeling of great historical tsunamis, we fill in this gap to determine which places are protected and which ones are liable to tsunamis. We also show which types of earthquakes are dangerous for La Réunion. We have modeled 4 tsunamis coming from the 3 subduction zones (Java, Sumatra and Makran) and studied the impact on the island and more precisely on 3 sites: Saint-Paul, Le Port Est and La Pointe des Galets harbours in the city of Le Port. In terms of amplitude, we note that a model using a complex seismic source with multiple subplans (model from Sladen and Hébert, 2008) better represents the real tsunami signal than a model using a simple seismic source (model from Hébert et al., 2007).

Our models show that the most destructive tsunamis in La Réunion are generated along the Sumatra subduction zone. The position along this subduction zone is also important. The 1833 event is used to determine the worst tsunami impact in La Réunion. Indeed, earthquakes situated in the south part of Sumatra induce a tsunami propagation more direct on La Réunion. For a similar magnitude earthquake (M_w = 9.2), the northern earthquake (2004 event) induces strong currents in harbours and flooding limited to beaches whereas the southern earthquake (1833 event) induces strong currents and eddies in harbours and flooding of the southern district of Saint-Paul. The tsunami amplitude is twice as large in the case of 1833 event than during the 2004 event. For all models we note that the shallow bathymetric structures off the East coast of Le Port Est and off the North coast of La Pointe des Galets harbour amplify the tsunami;

NHESSD
1, 1823–1855, 2013

they imply maximum wave heights and flooding of these areas. Velocities are important in the harbours and are amplified at the entrance of basins. The 2004 scenario illustrates the most common effects that can be expected in the harbours as well as local inundation of beaches. The 1833 model provides a worst-case scenario and thus gives an estimation of the maximum impact that could be feared in La Réunion. The impacts would be material and human with capesized and broken boats in harbours and flooding of southern habitable areas of Saint-Paul which underlines the need for an implementation of a warning system for this town. This work together with the study of Sahal (2011) perm The results of the PREPARTOI project which is the compilation of this work and the permit the setting up of this warning system (Sahal and Morin, 2012) in the town of Saint-Paul. A technical and administrative intervention plan will decide what measures are to be taken for the protection of the population in case of another tsunami.

Acknowledgements. The authors wish to thank E. Okal for his dicussion of the far-field modeling in the Indian Ocean as well as PREPARTOI partners. Work of this paper was supported by PREPARTOI project and LRC (Laboratoire de Recherche Commun Yves Rocard, ENS Ulm Paris 5). This work was granted access to the HPC resources of CCRT under the allocation 2011-6702 made by GENCI (Grand Equipement National de Calcul Intensif).

References

Ammon, C. J., Kanamori, H., Lay, T., and Velasco, A. A.: The 17 July 2006 Java tsunami earthquake, Geophys. Res. Lett., 33, L24308, doi:10.1029/2006GL028005, 2006. 1830

Byrne, D., Sykes, L. R., and Davis, D. M.: Great thrust earthquakes and aseismic slip along the plate boundary of the Makran Subduction Zone, J. Geophys. Res., 97, 449–478, doi:10.1029/91JB02165, 1992. 1829

Choi, B. H., Pelinovsky, E., Kim, K. O., and Lee, J. S.: Simulation of the trans-oceanic tsunami propagation due to the 1883 Krakatau volcanic eruption, Nat. Hazards Earth Syst. Sci., 3, 321–332, doi:10.5194/nhess-3-321-2003, 2003. 1825

NHESSD

1, 1823–1855, 2013

Crank, J. and Nicolson, P.: A practical method for numerical evaluation of solutions of partial differential equations of the heat-conduction type, Math. Proc. Cambridge, 43, 50–67, doi:10.1017/S0305004100023197, 1947. 1827

Dunbar, P.: NOAA/WDC historical tsunami database, available at: http://www.ngdc.noaa.gov/hazard/tsu.shtml, last access: 2 July 2012, 2010. 1827

Heidarzadeh, M., Pirooz, M. D., Zaker, N. H., and Mokhtari, M.: Evaluating the potential for tsunami generation in southern Iran, International Journal of Civil Engineering (IJCE), 5, 312–329, 2007. 1829

Heinrich, P., Schindelé, F., Guibourg, S., and Ihmlé, P. F.: Modeling of the February 1996 peruvian tsunami, Geophys. Res. Lett., 25, 2687–2690, doi:10.1029/98GL01780, 1998. 1826

Hébert, H., Heinrich, P., Schindelé, F., and Piatanesi, A.: Far-field simulation of tsunami propagation in the Pacific Ocean: impact on the Marquesas islands (French Polynesia), J. Geophys. Res., 106, 9161–9177, doi:10.1029/2000JC000552, 2001. 1827

Hébert, H., Sladen, A., and Schindelé, F.: Numerical modeling of the great 2004 Indian Ocean tsunami: focus on the Mascarene islands, B. Seismol. Soc. Am., 97, 208–222, doi:10.1785/0120050611, 2007. 1826, 1827, 1829, 1830, 1833, 1838, 1845, 1848, 1849

Jackson, J. and McKenzie, D.: Active tectonics of the Alpine–Himalayan belt between western Turkey and Pakistan, Geophys. J. Int., 77, 185–264, doi:10.1111/j.1365-246X.1984.tb01931.x, 1984. 1829

Jaiswal, R. K., Rastogi, B. K., and Murty, T. S.: Tsunamigenic sources in the Indian Ocean, Science of Tsunami Hazards, 27, 32–53, 2008. 1828

Kopp, C., Fruehn, J., Flueh, E., Reichert, C., Kukowski, N., Bialas, J., and Klaeschen, D.: Structure of the Makran subduction zone from wide-angle and reflection seismic data, Tectonophysics, 329, 171–191, doi:10.1016/S0040-1951(00)00195-5, 2000. 1829

Lay, T., Kanamori, H., Ammon, C. J., Nettles, M., Ward, S. N., Aster, R. C., Beck, S. L., Bilek, S. L., Brudzinski, M. R., Butler, R., DeShon, H. R., Ekström, G., Satake, K., and Sipkin, S.: The great Sumatra–Andaman earthquake of 26 December 2004, Science, 308, 1127–1133, doi:10.1126/science.1112250, 2005. 1827

Lynett, P. J., Borrero, J. C., Weiss, R., Son, S., Grerr, D., and Renteria, W.: Observations and modeling of tsunami-induced currents in ports and harbors, Earth Planet. Sci. Lett., 327–328, 68–74, doi:10.1016/j.epsl.2012.02.002, 2012. 1836

Merrifield, M. A., Firing, Y. L., Aarup, T., Agricole, W., Brundrit, G., Chang-Seng, D., Farre, R., Kilonsky, B., Knight, W., Kong, L., Magori, C., Manurung, P., McCreery, C., Mitchell, W.,

NHESSD
1, 1823–1855, 2013

Pillay, S., Schindelé, F., Shillington, F., Testut, L., Wijeratne, E. M. S., Caldwell, P., Jardin, J., Nakahara, S., Porter, F., and Turetsky, N.: Tide gauge observations of the Indian Ocean tsunami, 26 December 2004, Geophys. Res. Lett., 32, L09603, doi:10.1029/2005GL022610, 2005. 1825

Natawidjaja, D. H., Sieh, K., Chlieh, M., Galetzka, J., Bambang, W. S., Cheng, H., Edwards, R. L., Avouac, J., and Steven, N. W.: Source parameters of the great Sumatran megathrust earthquakes of 1797 and 1833 inferred from coral microatolls, J. Geophys. Res., 111, B06403, doi:10.1029/2005JB004025, 2006. 1828

Okada, Y.: Surface deformation due to shear and tensile faults in a half-space, B. Seismol. Soc. Am., 75, 1135–1154, 1985. 1826

Okal, E. A. and Synolakis, C. E.: Far-field tsunami hazard from mega-thrust earthquakes in the Indian Ocean, Geophys. J. Int., 172, 995–1015, doi:10.1111/j.1365-246X.2007.03674.x, 2008. 1824, 1828

Okal, E. A., Sladen, A., and Okal, E. A.: Rodrigues, Mauritius, and Réunion islands field survey after the December 2004 Indian Ocean tsunami, Earthq. Spectra, 22, 241–261, doi:10.1193/1.2209190, 2006. 1824, 1825, 1829, 1831, 1837

Pararas-Carayannis, G.: The potential of tsunami generation along the Makran Subduction Zone in the Northern Arabian Sea, case study: the earthquake and tsunami of 28 November 1945, Science of Tsunami Hazards, 24, 358–384, 2006. 1829

Rabinovich, A. B., Thomson, R. E., and Stephenson, F. E.: The Sumatra tsunami of 26 December 2004 as observed in the North Pacific and North Atlantic oceans, Surv. Geophys., 27, 647–677, doi:10.1007/s10712-006-9000-9, 2007. 1825

Rajendran, C. P., Ramanamurthy, M. V., Reddy, N. T., and Rajendran, K.: Hazard implications of the late arrival of the 1945 Makran tsunami, Curr. Sci. India, 95, 1739–1743, 2008. 1829, 1830, 1845

Rastogi, B. K. and Jaiswal, R. K.: A catalog of tsunamis in the Indian Ocean, Science of Tsunami Hazards, 25, 128–142, 2006. 1827

Sahal, A.: Le risque tsunami en France: contributions méthodologiques pour une évaluation intégrée par scénarios de risque, Ph.D. thesis, Université Panthéon-Sorbonne-Paris, France, 1, 314 pp., 2011 (in French). 1839

Sahal, A. and Morin, J.: Effects of the October 25th, 2010 Mentawai tsunami in La Réunion island (France): observations and crisis management, Nat. Hazards, 62, 1125–1136, doi:10.1007/s11069-012-0136-2, 2012. 1825, 1839

NHESSD
1, 1823–1855, 2013

Sahal, A., Roger, J., Allgeyer, S., Lemaire, B., Hébert, H., Schindelé, F., and Lavigne, F.: The tsunami triggered by the 21 May 2003 Boumerdès-Zemmouri (Algeria) earthquake: field investigations on the French Mediterranean coast and tsunami modelling, Nat. Hazards Earth Syst. Sci., 9, 1823-1834, doi:10.5194/nhess-9-1823-2009, 2009. 1827

Sahal, A., Pelletier, B., Chatelier, J., Lavigne, F., and Schindelé, F.: A catalog of tsunamis in New Caledonia from 28 March 1875 to 30 September 2009, C. R. Geosci., 342, 434–447, 2010. 1827

Sahal, A., Morin, J., Schindelé, F., and Lavigne, F.: A catalog of tsunamis in La Réunion island from August 27th, 1883 to October 26th, 2010, Science of tsunami hazards, 30, 178–190, 2011. 1825

Schläter, H. U., Prexl, A., Gaedicke, C., Roeser, H., Reichert, C., Meyer, H., and von Daniels, C.: The Makran accretionary wedge: sediment thicknesses and ages and the origin of mud volcanoes, Mar. Geol., 185, 219–232, doi:10.1016/S0025-3227(02)00192-5, 2002. 1829

Sladen, A. and Hébert, H.: On the use of satellite altimetry to infer the earthquake rupture characteristics: application to the 2004 Sumatra event, Geophys. J. Int., 172, 707–714, doi:10.1111/j.1365-246X.2007.03669.x, 2008. 1827, 1829, 1830, 1833, 1834, 1838, 1845, 1846, 1848

Zachariasen, J., Sieh, K., Taylor, F. W., Edwards, R. L., and Hantoro, W. S.: Submergence and uplift associated with the giant 1833 Sumatran subduction earthquake: evidence from coral microatolls, J. Geophys. Res., 104, 895–920, doi:10.1029/1998JB900050, 1999. 1828, 1830, 1834, 1843, 1845, 1848, 1850, 1851, 1852, 1853, 1854

NHESSD
1, 1823–1855, 2013

Table 1. Seismic source parameters for the 1833 event from Zachariasen et al. (1999). Lon. and Lat. are the coordinates of the epicenter, z the depth fault, d the coseismic displacement. The fault geometry is given by its strike, dip and rake angles and by its length (L) and width (W). μ is the rigidity.

Lon.	Lat.	z (km)	d (m)	strike	dip	rake	L (km)	W (km)	μ (N m^2)
100.45	−3.25	35	26	322	14	90	550	250	2E+10

NHESSD
1, 1823–1855, 2013

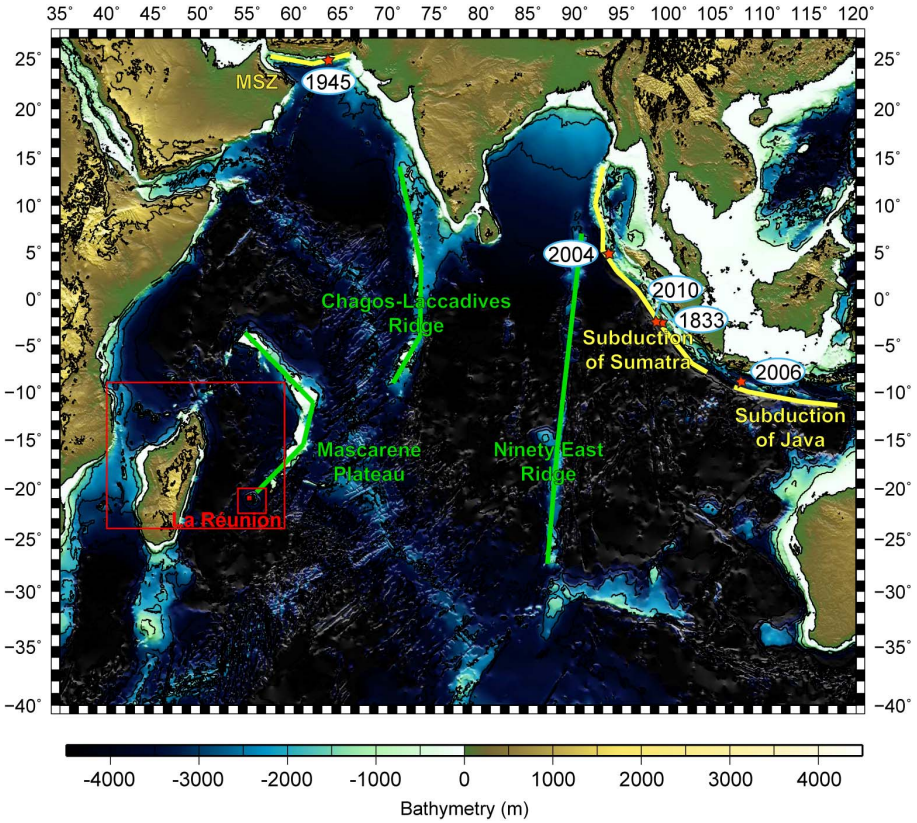

Fig. 1. Context of the study in the Indian Ocean with the focus on La Réunion Island (Red rectangles). The tsunamigenic seismic structures are highlighted in yellow: Java, Sumatra and Makran (MSZ) subduction zones. The reliefs of the seafloor are underlined in green: Chagos-Laccadive Ridge, Mascarene Plateau and Ninety East Ridge.

NHESSD
1, 1823–1855, 2013

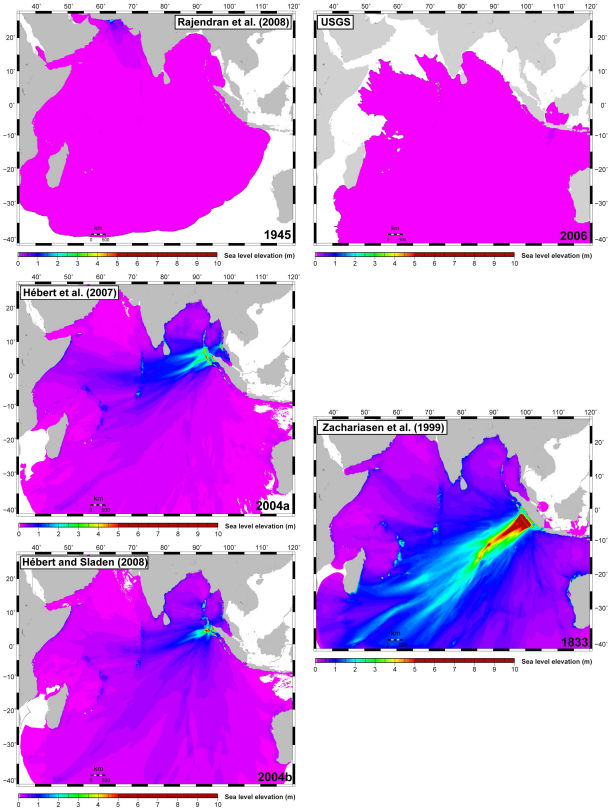

Fig. 2. Maximum water heights (in m) for 1945 (Rajendran et al., 2008), 1833 (Zachariasen et al., 1999), 2004a (Hébert et al., 2007) and 2004b (Sladen and Hébert, 2008) and 2006 (USGS) events after 10 h of propagation.

NHESSD
1, 1823–1855, 2013

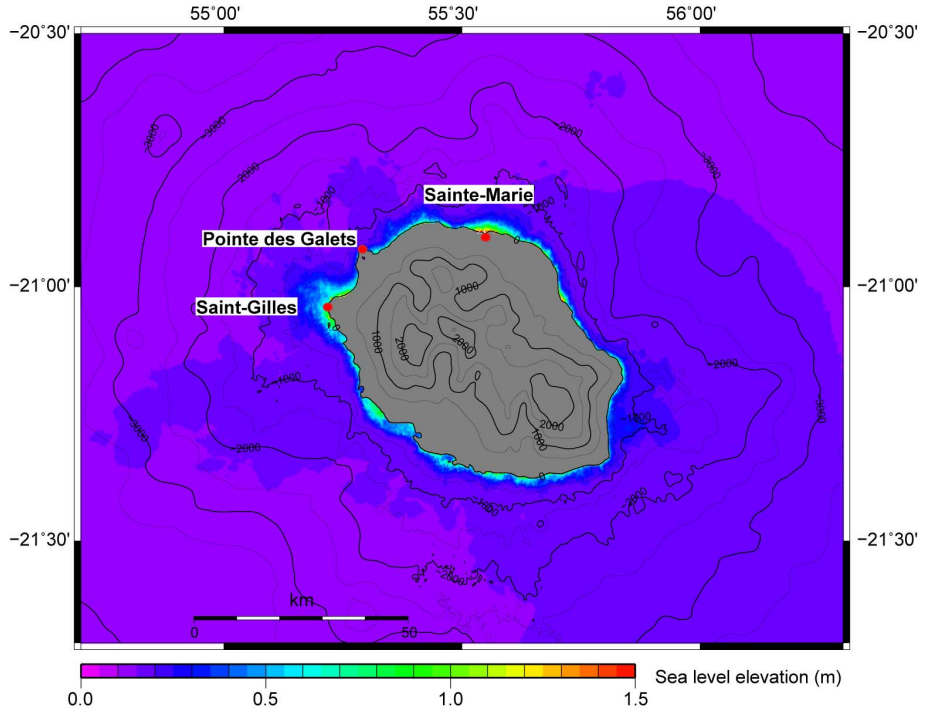

Fig. 3. Maximum water heights (in m) in La Réunion island for 2004 event after 9 h of propagation for the source model of Sladen and Hébert (2008).

NHESSD
1, 1823–1855, 2013

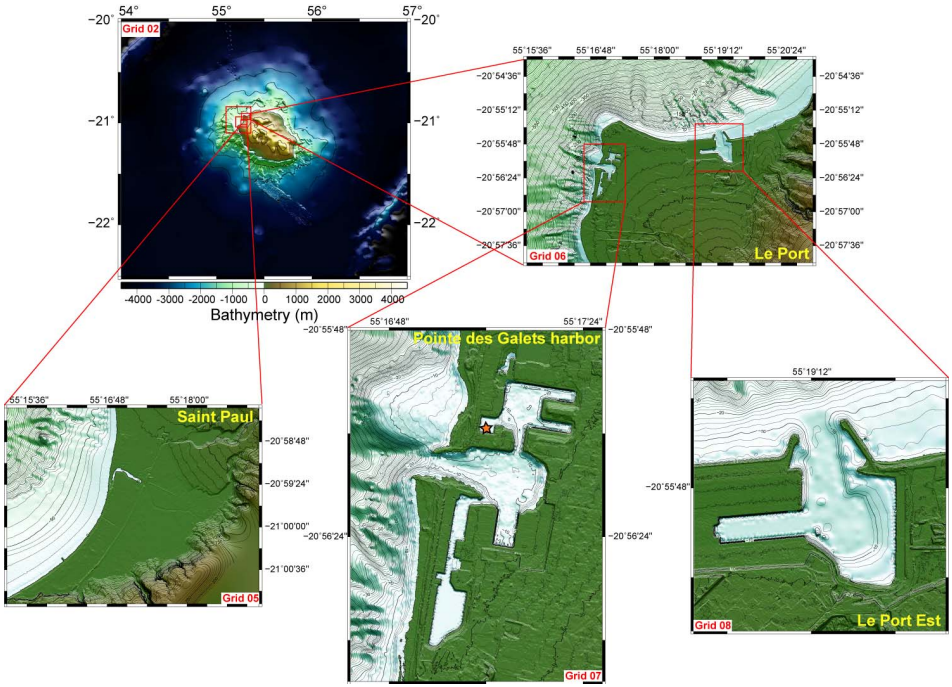

Fig. 4. Location of La Réunion study sites and modeling grids; Grid02 (300 m resolution) is centered on La Réunion island, Grid05 (4 m resolution) on Saint-Paul, Grid06 (12 m resolution) on Le Port town, Grid07 and Grid08 (3 m resolution) on its two harbours, La Pointe des Galets and Le Port Est. The red star shows the tide gauge location.

NHESSD
1, 1823–1855, 2013

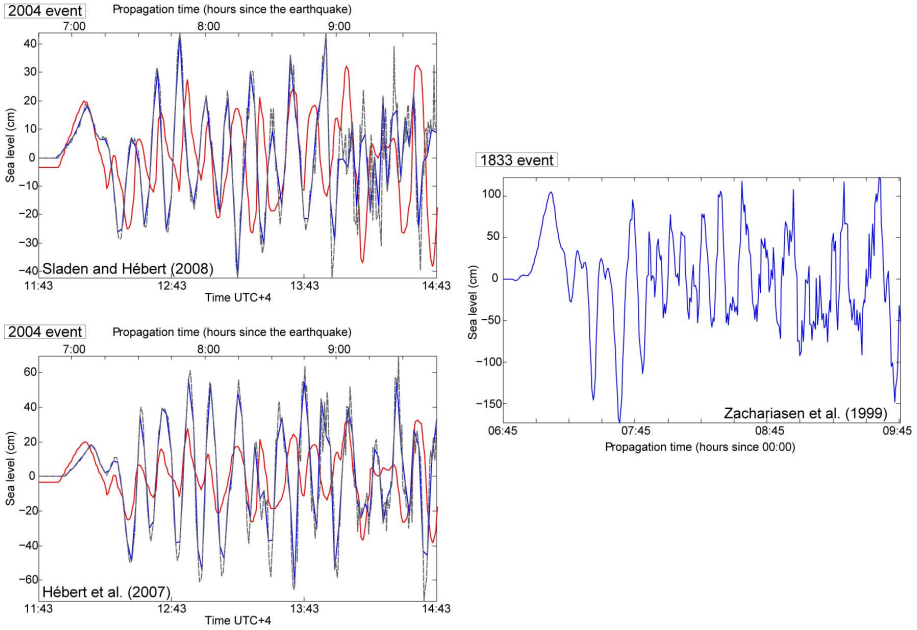

Fig. 5. Observed (red) and synthetic (dotted gray) maregrams comparison of La Réunion for, at left, the 2004 event using the source models from Sladen and Hébert (2008) and Hébert et al. (2007) and for, at right, the 1833 event using the source model from Zachariasen et al. (1999). The blue curve is the simulated signal, filtered with the tide gauge sample rate (2 min).

NHESSD
1, 1823–1855, 2013

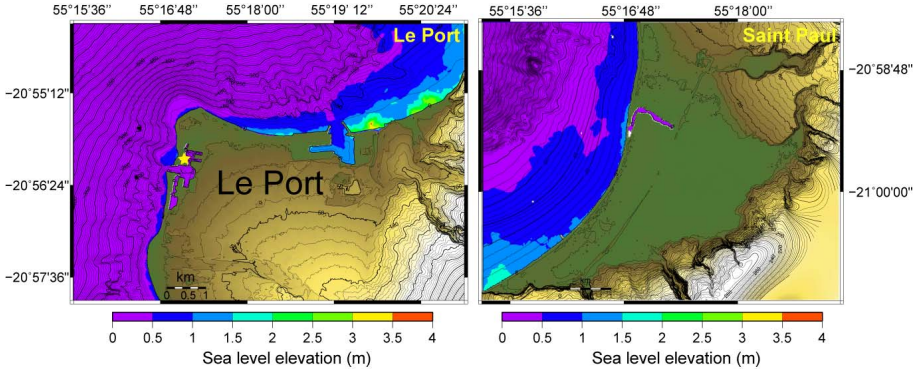

Fig. 6. Maximum water heights for the 2004 event in Le Port and Saint-Paul using the source model from Hébert et al. (2007). The yellow star shows the tide gauge location.

NHESSD
1, 1823–1855, 2013

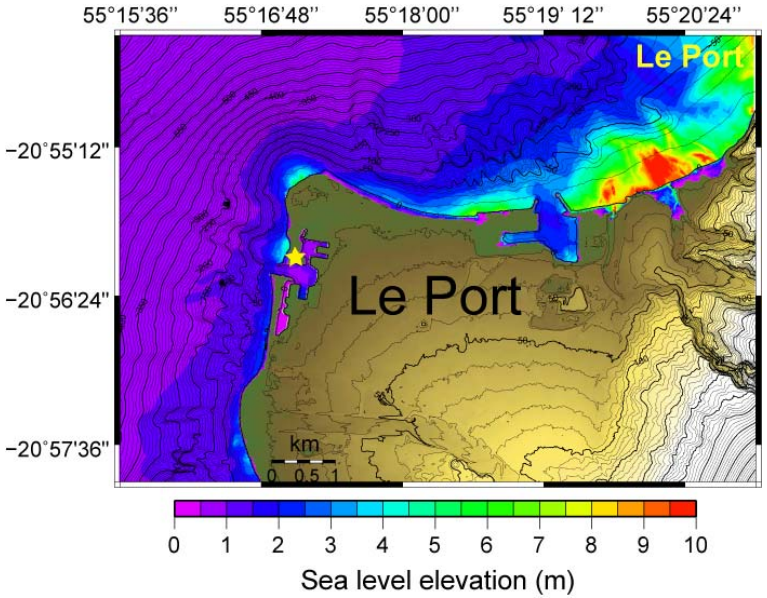

Fig. 7. Maximum water heights for the 1833 event in Le Port using the source model from Zachariasen et al. (1999). The yellow star shows the tide gauge location.

NHESSD
1, 1823–1855, 2013

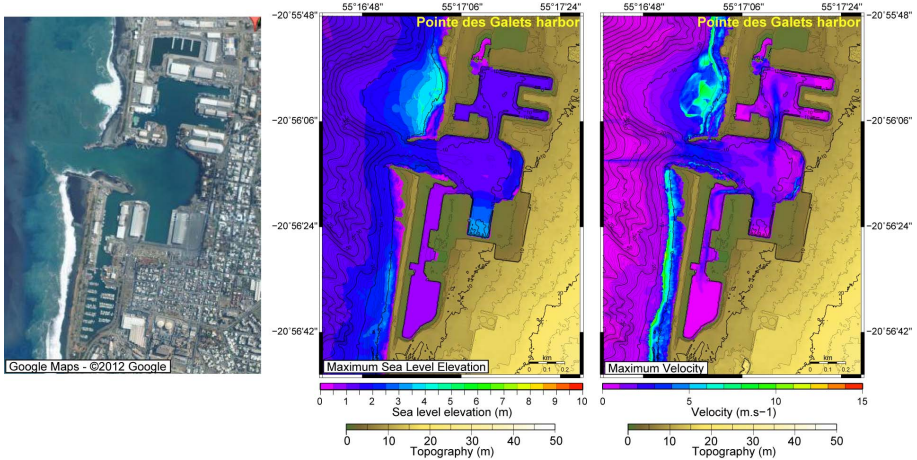

Fig. 8. Maximum water heights and maximum velocities for La Pointe des Galets harbour using the source model from Zachariasen et al. (1999), 1833 event.

NHESSD
1, 1823–1855, 2013

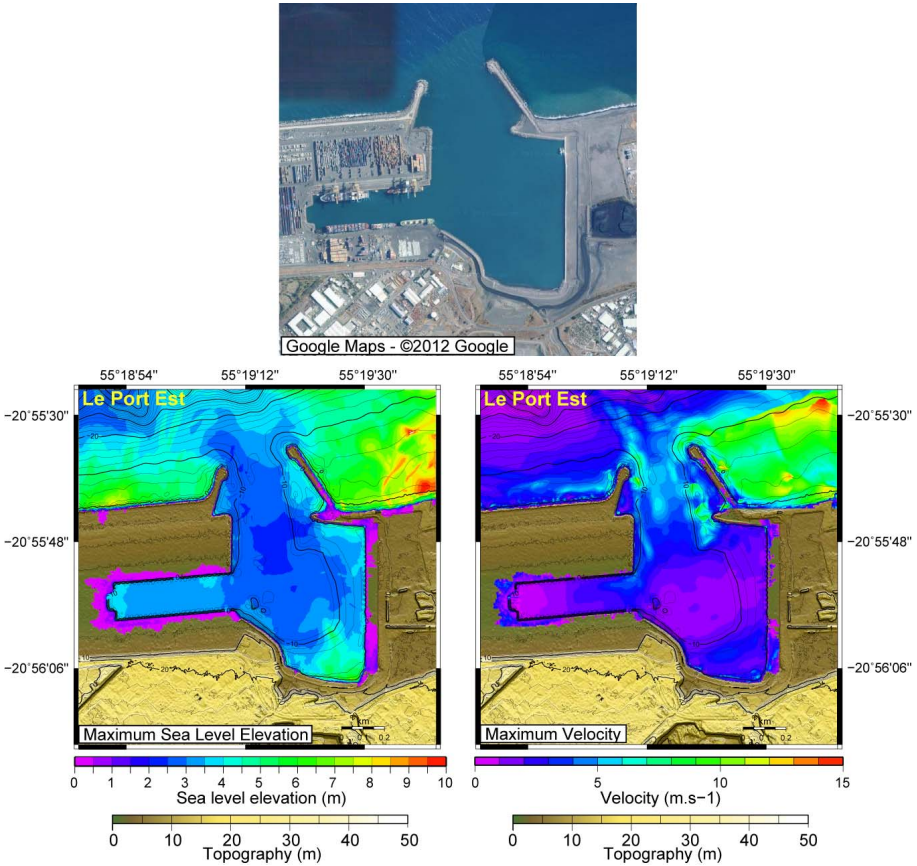

Fig. 9. Maximum water heights and maximum velocities for Le Port Est for the 1833 event using the source model from Zachariasen et al. (1999).

NHESSD
1, 1823–1855, 2013

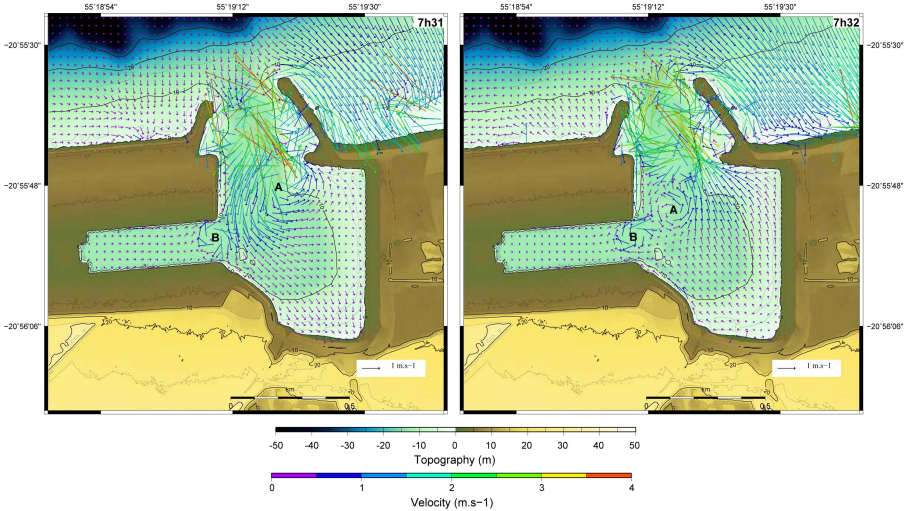

Fig. 10. Velocity field in Le Port Est for the 1833 event using the source model from Zachariasen et al. (1999).

NHESSD
1, 1823–1855, 2013

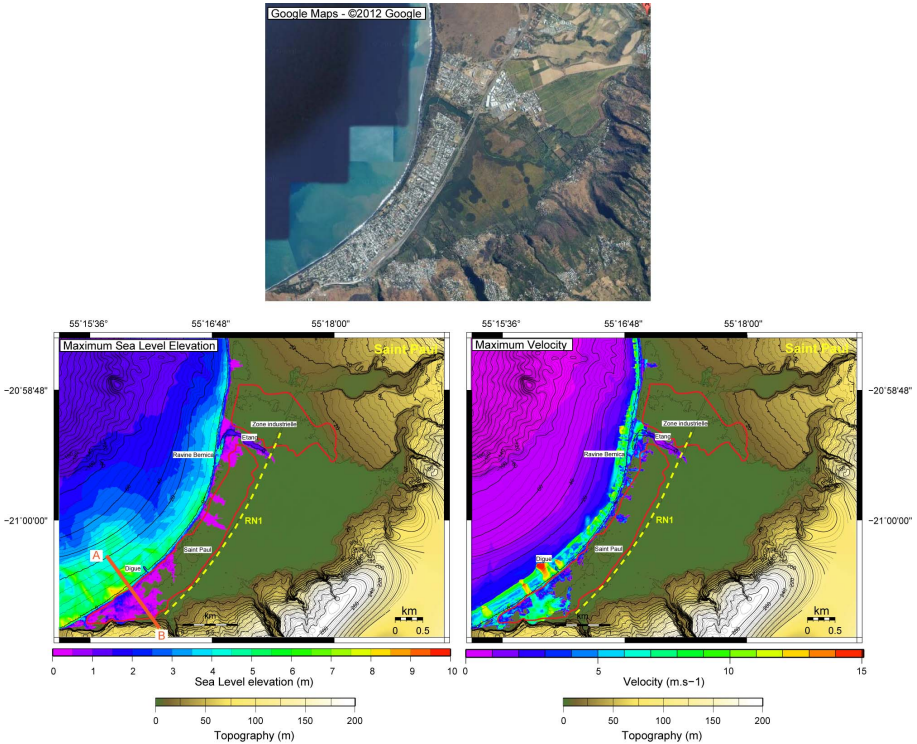

Fig. 11. Maximum water heights and maximum velocities at Saint-Paul for the 1833 event using the source model from Zachariasen et al. (1999). The red line shows the flooding extension.

NHESSD
1, 1823–1855, 2013

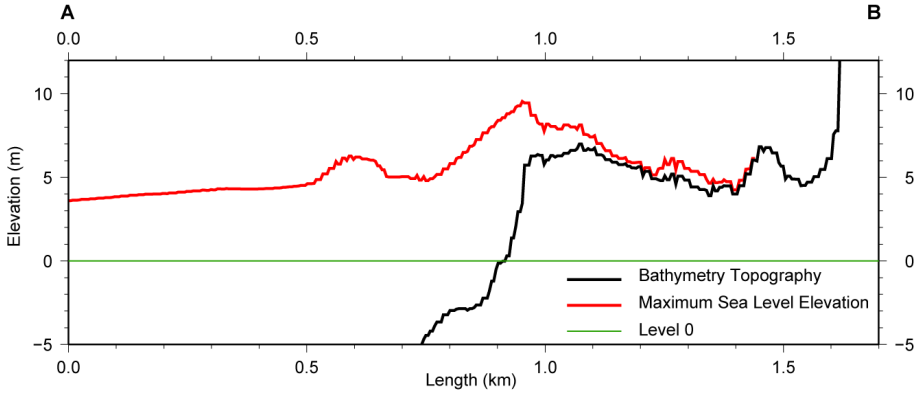

Fig. 12. Maximal water heights profile across the southern coastal area of Saint-Paul for the 1833 event (location on Fig. 11); the red curve is the sea level elevation, the black one the bathymetric and topographic profile and the green line the 0 m level.

NHESSD
1, 1823–1855, 2013